

Green Chemistry

Accepted Manuscript



This is an *Accepted Manuscript*, which has been through the Royal Society of Chemistry peer review process and has been accepted for publication.

Accepted Manuscripts are published online shortly after acceptance, before technical editing, formatting and proof reading. Using this free service, authors can make their results available to the community, in citable form, before we publish the edited article. We will replace this *Accepted Manuscript* with the edited and formatted *Advance Article* as soon as it is available.

You can find more information about *Accepted Manuscripts* in the [Information for Authors](#).

Please note that technical editing may introduce minor changes to the text and/or graphics, which may alter content. The journal's standard [Terms & Conditions](#) and the [Ethical guidelines](#) still apply. In no event shall the Royal Society of Chemistry be held responsible for any errors or omissions in this *Accepted Manuscript* or any consequences arising from the use of any information it contains.

Room Temperature Selective Oxidation of Aniline to Azoxybenzene over Silver supported Tungsten Oxide Nanostructured Catalyst †

Shilpi Ghosh, Shankha S. Acharyya, Takehiko Sasaki and Rajaram Bal*

Abstract

Heterogeneous catalysts comprising of silver nanoparticles supported on nanostructured tungsten oxide were applied for the room temperature oxidative coupling of aniline to azoxybenzene, an important chemical intermediate and a chemical of industrial interest. The catalytic protocol features high activity and selectivity to the target product azoxybenzene with a turn over number of ~368. The catalyst was characterized by XRD, XPS, ICP-AES, FT-IR, TGA, EXAFS, SEM and TEM. The silver-tungsten nanomaterial acts as an excellent catalyst for selective oxidation of aniline to azoxybenzene using H₂O₂ as an oxidant. An aniline conversion of 87% with 91% selectivity of azoxybenzene was achieved without the use of any external additives. Moreover, a high stability and recyclability of the catalyst is also observed under the investigated conditions.

1. Introduction

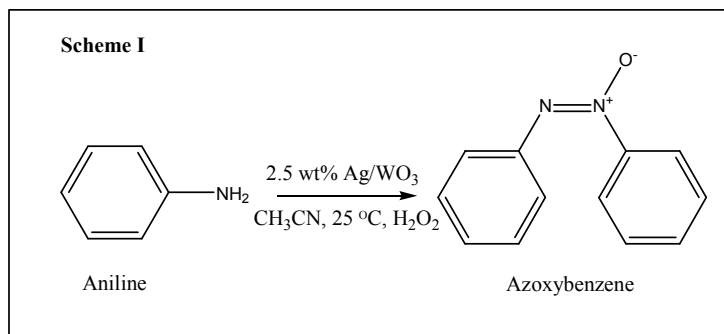
Now-a-days growing attention is being directed towards the development of superior catalytic systems with high performance from the view points of environmentally greener process, economical efficiency and minimum consumption of resources. Nanostructured materials are potential candidates because of their unique properties they exhibit, are different compared to their bulk counterparts.¹⁻⁴ Nanomaterials with controlled size and well-defined shapes are promising candidates for catalysis as these materials could facilitate the control of

tuning the catalytic properties. It is a well known phenomenon that both catalytic efficiency and selectivity are highly dependent on the size and shape of the nanostructure materials and the composition of the metals and support used.⁵ Therefore, the synthesis of nanomaterials with specific morphology has sparked growing interest in the field of catalysis over the past years. Simple preparation methods are required for easy manipulation of the nucleation and growth kinetics to give a tunable shape and size of the nanoparticles. We report here the simple preparation of very small Ag nanoparticles supported on nanocrystalline WO₃. This procedure is highly reproducible and large quantity (~30 g) material can be prepared.

Oxidation reactions are of fundamental importance in nature. Selective catalytic oxidation of aniline is an important reaction for the synthesis of intermediates and a precursor to various industrially valuable oxygenated products such as nitrobenzene, nitroso benzene, azo benzene and azoxy benzene.⁶ Azoxy benzene is one of the most important and central building blocks in naturally occurring compounds and functional materials.⁷ It is valuable both as intermediates and high value compounds such as dyes, reducing agents, chemical stabilizers and polymerisation inhibitors.⁸ Moreover, azoxybenzene is the precursor for Wallach rearrangement, which offers a simple way to prepare hydroxyazobenzene.^{9,10} Therefore, the challenge lies in controlling the selectivity to the target product in the midst of all possible oxidation products at a reasonable substrate conversion in order to meet the market needs. Various attempts were made for oxidative coupling of aniline using different oxidants like peracetic acid,¹¹ Pb(OAc)₄,¹² Hg(OAc)₂¹³ and BaMnO₄¹⁴ but the employment of these oxidants lacks environmental benignity. Molybdenum and vanadium-compounds catalyze aniline oxidation in presence of *tert*-butyl hydrogen peroxide (TBHP).¹⁵ The use of TBHP is cost effective as compare to H₂O₂ and suffers from environmental problem. So, finding the alternative, more benign methods of producing azoxybenzene with high conversion and selectivity, with the aid of environmentally clean and cheaper oxidants like molecular oxygen

or H_2O_2 is highly desirable. Applications of molecular oxygen and hydrogen peroxide as oxidizing agents for selective oxidation of aniline in industry will have immense potential interest. Recent years we have witnessed tremendous progress in selective oxidation of aromatic amines. Hydrogen peroxide in presence of rhenium, tungsten or molybdenum catalysts also gives nitrosoarenes with high yields.¹⁶⁻¹⁸ Silica containing cobalt oxide catalyst is reported to catalyse this reaction selectively at comparatively higher temperature (80 °C) using H_2O_2 as oxidant.¹⁹ Titanium silicate molecular sieves, TS-1 as catalyst affords selective oxidation of aniline to nitrosobenzene using H_2O_2 as oxidant.²⁰ Recently, spinel CuCr_2O_4 nanocatalyst was found to be suitable for oxidation of aniline to azoxybenzene at 70° C with 78% aniline conversion and 92% azoxybenzene selectivity.⁸ Corma et al. reported a Au/TiO_2 to catalyse aerobic oxidation aniline to azobenzene very selectively.²¹ Li et al. reported Ag nanoparticles catalysed selective aerial oxidation of aniline to azobenzene in presence of dimethyl sulfoxide as solvent in presence of KOH as a base at room temperature.²² Heteropolyoxometalates ($\text{H}_3\text{PW}_{12}\text{O}_{40}$) are also reported to catalyse aniline to nitrosobenzene and nitrobenzene reaction at room temperature in presence of dichloromethane.²³ Although various catalysts have been efficiently used for the preparation of azoxybenzene, but a successful catalytic system with very high selectivity and yield of azoxybenzene using environmentally benign oxidant at room temperature has not been achieved. So, the development of heterogeneous catalyst for selective oxidation of aniline to azoxybenzene under mild condition is highly demanding.

We report here the preparation of ~2-5 nm Ag nanoparticles supported on nanocrystalline WO_3 for the selective oxidation of aniline to azoxybenzene at room temperature (25° C) (see scheme I). An aniline conversion of 87% with 91% azoxybenzene selectivity was achieved at room temperature with a turn over number of ~368.



2. Experimental

2.1 Materials

Ammonium metatungstate hydrate, AgNO_3 , cetyltrimethylammonium bromide, HPLC grade (~99.9%) aniline, acetonitrile were purchased from Sigma-Aldrich Co. Hydrogen Peroxide (50 wt % in water) was purchased from Merck KGaA, Darmstadt, Germany. All the chemicals were used without further purification. Double distilled water was used during the preparation of catalyst.

2.2 Preparation of Ag/WO_3 nanostructured catalyst

The catalyst was prepared by modified our own preparation method.²⁴ The advantage of this method is that the catalyst was prepared at room temperature without the addition of hydrazine. AgNO_3 , ammonium metatungstate hydrate, cetyltrimethylammonium bromide (CTAB) was mixed maintaining a molar ratio of $\text{Ag}:\text{CTAB}:\text{H}_2\text{O} = 1:0.70:800$. In a typical synthesis method, an aqueous solution of 0.32 g AgNO_3 was added to 12.8 g ammonium metatungstate hydrate solution at room temperature with vigorous stirring for 1 h. Then 0.5 g CTAB solution was added dropwise. The mixture was stirred for another 3 h. After that the product was filtered, washed with ethanol and dried at 110 °C for 12 h and finally heated at 500°C for 6 h in presence of helium.

Catalyst Characterization

A thorough characterization of the catalyst was done using different characterization techniques like XRD, ICP-AES, SEM, TEM, BET surface area, EXAFS, XPS and TGA. Powder X-ray diffraction patterns were collected on a Bruker D8 advance X-ray diffractometer fitted with a Lynx eye high-speed strip detector and a Cu K α radiation source. Diffraction patterns in the 2°-80° region were recorded at a rate of 0.5 degrees (2 θ) per minute. Scanning electron microscopy (SEM) images were taken on a FEI Quanta 200 F, using tungsten filament doped with lanthanumhexaboride (LaB $_6$) as an X-ray source, fitted with an ETD detector with high vacuum mode using secondary electrons and an acceleration tension of 10 or 30 kV. Samples were analyzed by spreading them on a carbon tape. Energy dispersive X-ray spectroscopy (EDX) was used in connection with SEM for the elemental analysis. The elemental mapping was also collected with the same spectrophotometer. TEM images were collected using a JEOL JEM 2100 microscope, and samples were prepared by mounting an ethanol-dispersed sample on a lacey carbon formvar coated Cu grid. X-ray photoelectron spectroscopy (XPS). X-Ray photoelectron spectra were recorded on a Thermo Scientific K-Alpha X-Ray photoelectron spectrometer and binding energies (± 0.1 eV) were determined with respect to the position C 1s peak at 284.8 eV. Raman spectra was measured at 298K by using a Laser Raman Spectrometer (JASCO, NRS-3100) with the 532 nm line from a diode-pumped solid-state laser for excitation. Measurements of extended X-ray absorption fine structure (EXAFS) at Ag-K edge were carried out in a transmission mode at room temperature at the NW10A station of the Photon Factory- Advanced Ring for pulse X-Rays at the Institute of Materials Structure Science, High Energy Accelerator Research Organization in Japan (KEK-IMSS-PF-AR). The electron storage ring was operated at 6.5 GeV. Synchrotron radiation from the storage ring was monochromatized by a Si (311) channel cut crystal at Ag K-edge. Ionization chambers, which were used as detectors for

incident X-ray (I_0) and transmitted X-ray (I), were filled with 50% Ar/N₂ mixture gas and 100 % Ar gas, respectively. The EXAFS raw data were analyzed with UWXAFS analysis package,²⁴ including background subtraction program AUTOBK,²⁵ curve fitting program FEFFIT.²⁶ The amplitude reducing factor S_0^2 for Ag was fixed at 0.95. The backscattering amplitude and phase shift were calculated theoretically by FEFF 8.4 code.²⁷ ATOMS²⁸ was used to obtain the FEFF input code for crystalline materials. Chemical analyses of the metallic constituents were carried out by Inductively Coupled Plasma Atomic Emission Spectrometer; model: PS 3000 uv, (DRE), Leeman Labs, Inc, (USA). Fourier Transformation Infra-red Spectroscopy (FTIR) spectra were recorded on a Thermo Nicolet 8700 (USA) instrument with the operating conditions: resolution: 4cm⁻¹, scan: 36, operating temperature: 23-25°C and the frequency range 4000-400 cm⁻¹. Thermogravimetric Analyses (TGA) of the uncalcined catalyst were carried out in a Pyris Diamond, Perkin Elmer instruments, and technology by SII (Seiko Instruments Inc), USA] instrument-balance by heating 2.15 mg samples at 5 °C min⁻¹ in flowing nitrogen.

Catalytic Oxidation of Aniline

Liquid phase oxidation of aniline was carried out at room temperature (25 °C) in a double neck round bottom flask at room temperature in an oil bath using 0.10 g catalyst, 10 ml acetonitrile solvent and 1 g of aniline to which 2.15 g H₂O₂ (50% aq. solution) was added dropwise. Small aliquots of the sample were withdrawn from the reaction mixture at regular intervals for analysis. At the end of the reaction, the solid particles (catalyst) were separated by filtering during the hot condition and products were analysed by gas chromatograph (GC, Agilent 7890) connected with a HP-5 capillary column (30 m length, 0.28 mm id and 0.25 µm film thickness) and a flame ionization detector (FID). Conversion of aniline was

calculated based upon the GC-FID results, where aniline conversion = [moles of aniline reacted]/[initial moles of aniline used] x 100 and selectivity of products calculated by [total moles of product formed]/[total moles of aniline converted] x 100. The individual yields were calculated and normalized with respect to the GC response factors. The product identification was carried out by injecting authentic standard samples in GC and GCMS. For few cases, we did the column chromatography to get the isolated yield and $^1\text{H-NMR}$ was taken to identify the product. The C-balance as well as material balance was carried out for most of the experiments and it was found between 98-102%. For the reusability test, after completion of the reaction, the catalyst was recovered from the reaction mixture by filtration and washed thoroughly with acetone and reused as such for multiple cycles.

RESULTS AND DISCUSSIONS

Catalyst characterization

The amount of silver present in the Ag/WO₃ nanostructured catalyst was estimated by ICP-AES. The related X-ray diffraction (XRD) pattern of the Ag/WO₃ nanostructured catalyst showed the peaks at 2 θ values of 23.1°, 23.7°, 24.4°, 33.3° and 34.0°, confirm the formation of monoclinic WO₃ (JCPDS No. 43-1035, space group: P21/n) (Fig.1). However, we could not observe any diffraction peaks assignable to metallic silver Ag (0) or oxides of silver, indicating the very small silver particles size (2-5 nm). X-ray photoelectron spectroscopy (XPS) analyses clearly the presence of metallic silver in the fresh sample from the corresponding Ag 3d_{5/2} and Ag 3d_{3/2} binding energy values of 368.2 eV and 374.1 eV respectively (Fig. 2).²⁹ The W 4f_{5/2} and 4f_{7/2} spectra attributed to the binding energies 37.9 eV and 35.8 eV respectively suggesting that the tungsten in the tungsten oxide sample exists as W⁺⁶.³⁰ (Fig. 3) The corresponding Ag 3d binding energy of the spent catalyst ~368.3 eV, confirms that the oxidation state of metallic silver does not change during catalysis. (Fig.2b).

The representative SEM images of the catalyst are shown in Fig. 4. The images showed that the Ag/WO₃ nanostructured catalyst is comprised of very small particles. The SEM elemental mapping exhibits a uniform dispersion of silver nanoparticles on WO₃ support (Fig. S1). The electron diffraction (ED) pattern showed only the presence of silver, oxygen and tungsten and no impurities could be observed in the spectra (Fig.4c). Transmission electron microscopy (TEM) measurements were carried out to check the particle size and distribution of the silver nanoparticles (Fig 5). High resolution transmission electron microscopy (HRTEM) revealed that the catalyst is composed of highly dispersed very small silver nanoparticles of ~2-5 nm on WO₃ support. The corresponding TEM histogram of Ag nanoparticles showed a very narrow particle size distribution with sizes between 2-5 nm (Fig 4b, inset). The lattice fringe distance of 0.38 nm indicates the [020] lattice spacing of WO₃ and the distance of 0.20 nm corresponds to [200] plane of Ag (Fig. 3d). SAED pattern (Fig. 5c) exhibited the inter planar spacing distances of 0.23 nm, 0.20 nm and 0.14 nm, these are indexed to Ag (111), (200) and (220) respectively, which refer to the unique characteristic of the fcc structure of Ag. The lattice fringes with a d-spacing of 0.38 nm, 0.37 nm and 0.26 nm were also observed in the SAED pattern which corresponds to (002), (020) and (022) lattice planes of WO₃ with monoclinic structure. The TEM elemental mapping indicates the presence of Ag, W and O species and further ascertains the uniformly dispersion of AgNPs on tungsten oxide support (Fig 6). Furthermore, the TEM image of the spent catalyst showed that the topology and the silver particle size of the catalyst were hardly changed after four reuses (Fig 5e, f). TEM EDX pattern also showed the presence of Ag and W in the sample (Fig. S2). The surface area of the fresh Ag/WO₃ and spent Ag/WO₃ were 50 m²/g and 47 m²/g respectively, which also indicates that the available active sites remained constant during the catalysis. Ag-K edge extended X-ray absorption fine structure (EXAFS) analysis of the Ag/WO₃ nanostructure catalyst further revealed that no significant changes occurred in oxidation state of the silver

species of the fresh and the spent Ag/WO₃ nanostructure catalyst during the oxidative coupling of aniline to azoxybenzene (Table 1, Fig. S3). Table 1 shows the structural parameters of the catalyst by curve-fitting of the Ag K-edge EXAFS data. It was observed that Ag-Ag contribution at 0.2872 nm with a coordination number (C.N.) of 6.3 and the absence of Ag-O contribution indicates the formation of metallic Ag in the fresh catalyst. For the spent catalyst, Ag-Ag bond at 0.2873 nm with C.N. 7.7 was observed. The observation indicated that the oxidation state of Ag (0) remained unchanged after the catalysis which was supported by XPS also. The embedment of the cetyltrimethyl ammonium bromide molecules over the precalcined catalyst was confirmed by the FTIR analysis (see Figure 7). The peaks of the sample at 811 and 1099 cm⁻¹ can be assigned to the C-N⁺ stretching modes of CTA molecules. The peaks at 1361 cm⁻¹ are assigned to the symmetric mode of vibration of the head groups of the methylene moiety (N⁺-CH₃).³¹ The frequencies above 1600 cm to 3000 cm⁻¹ are due to CH symmetric and antisymmetric vibrations, respectively. The characteristic peaks at 628, 890 cm⁻¹ represent the stretching vibration of W-O-W and the peak at 948 cm⁻¹ associated with the stretching vibration of W=O.³² The embedment of CTAB molecules on the pre-calcined catalyst surface was further confirmed from TGA analysis. TGA analysis was operated to understand the various decomposition regimes as shown in Fig. 8. The TGA diagram showed that the weight loss has two regimes, first being the ~ 3% mass loss of water at 200 to 300 °C and finally the major mass loss of 12% around 450 °C is assigned to the decomposition of CTA moiety. Further weight loss was not observed when the temperature was further increased from 500°-700° C, indicating the stability of the catalyst upto 700° C. Total mass reduction of ~15% confirmed the complete the removal of the surfactant CTAB. UV-vis DRS of the Ag/WO₃ catalyst in Fig. 9 showed an absorption maxima at 401 nm. According to literature, the oxygen ligand to metal charge transfer (LMCT) bands for W⁺⁶, appeared ~300-400 nm.³³ The UV-vis absorption spectra of silver nanoparticles occurs ~410

nm.³⁴ Therefore, the absorption maxima ~ 401 nm could be assigned to the presence of both silver and WO_3 nanoparticles.

Catalytic Activity

We have investigated the catalytic activity of Ag/WO_3 nanostructured catalyst towards the oxidative coupling of aniline to azoxybenzene at room temperature and at atmospheric pressure using acetonitrile as solvent and H_2O_2 as an oxidizing agent. The results showed that the Ag/WO_3 nanostructured catalyst afforded an azoxybenzene selectivity of 91% with an aniline conversion of $\sim 87\%$ under catalyst/aniline weight ratio of 1:10 and aniline: H_2O_2 molar ratio of 1:3. Nitroso benzene, nitrobenzene and azo benzene were detected as the side products of this reaction. A series of catalytic experiment was carried out using Ag/WO_3 nanostructured catalyst in order to understand the variation of aniline to azoxybenzene conversion as a function of time, temperature and aniline: H_2O_2 mole ratio. The catalyst exhibits an aniline conversion of 87% at room temperature with azoxybenzene selectivity of 91%. We observed that with the increase of temperature although the conversion increases steadily but the selectivity drops down due to the formation of nitrobenzene as the major side product (Fig. 10). The results also showed an increasing trend in both the aniline conversion as well as azoxybenzene selectivity with increase of time (Fig. 11). After 6h of reaction, the catalyst exhibited an aniline conversion of 38% with 63% azoxybenzene selectivity; nitroso benzene was found to be the major side product. The results indicated that after 24 h of reaction, maximum selectivity of azoxybenzene ($\sim 91\%$) was achieved, but after 30 h, the selectivity of azoxybenzene drops down to $\sim 78\%$ due to formation of nitrobenzene. The mole ratio of aniline: H_2O_2 was used in three fold excess (Fig. 12). In fact when aniline: H_2O_2 was adjusted to 1:1, the conversion of aniline was very low (25%) with azoxybenzene selectivity $\sim 63\%$ and nitrosobenzene selectivity $\sim 35\%$. But when aniline : H_2O_2 mole ratio was

increased to 1:3, aniline conversion increases to 87 % with 91% azoxybenzene selectivity, further increase in the aniline : H₂O₂ mole ratio to 1:5, we noticed that although the aniline conversion increased to 93% but the azoxybenzene selectivity decreased significantly to 70%, owing to the formation of nitrobenzene as the major side product. Table 2 showed the activity of the different Ag/WO₃ catalysts in the selective oxidation of aniline to azoxybenzene in liquid phase using H₂O₂ as oxidant. The Ag/WO₃ nanostructured catalyst showed 87% aniline conversion and ~91% azoxybenzene selectivity with turn over number (TON) value of ~ 367.8 in the absence of any external additives at room temperature (Table 2, entry 6). Blank run in the absence of the catalyst gave almost no reactivity under the optimized reaction condition (Table 2, entry 8). Ag/WO₃ nanostructured catalyst prepared by surfactant promoted method provided excellent yield of azoxybenzene (Table 2, entry 6). When Ag/WO₃ catalyst synthesized by the conventional impregnation method, it showed very poor catalytic activity due to the irregular shape and larger particle sizes and excessive leaching of the metals (Table 1, entry 5). So, particles in the nanodomain definitely have a role towards the higher catalytic efficiency. Furthermore, Ag/WO₃ nanostructured catalyst showed greater TON of 367.8 for azoxybenzene production and greater H₂O₂ efficiency of ~26.4%, compared to alone Ag or WO₃ catalyst prepared through surfactant promoted method (Table 2, entries 3, 4). Results showed that when Ag, prepared by surfactant assisted method, was exclusively employed as catalyst, selective formation of azobenzene as the principal product was observed under the identical reaction conditions, with a lower aniline conversion of 37%. Notably WO₃ catalyst, prepared by surfactant promoted method, was also capable of selectively catalyzing aniline to azoxybenzene with 30.7% yield. Although Ag and WO₃ catalysts exhibited different catalytic profiles, these results further indicated a clear participation of both Ag and WO₃ species in the Ag/WO₃ nanostructured catalyst during the oxidative coupling of aniline under the investigated conditions. We believe that a synergistic

effect between the support WO_3 and Ag nanoparticles may exist at the interface, which further confirms that WO_3 does not simply act as a support, but also intervenes in the catalytic process.

To illustrate the general applicability of Ag/ WO_3 nanostructured catalyst, the scope of the reaction was extended to oxidative coupling of a range of aromatic amines (Table 3). Under the optimized conditions, we found that a variety of structurally different aromatic amines were selectively transformed to their corresponding azoxy products with high yield.

The mechanism of the reaction was supposed to follow the path as shown in scheme S1. We believe that the initial step is the decomposition of H_2O_2 over AgNPs to form superoxide ($\text{O}_2^{\bullet-}$), according to the reaction shown in eq (i) in the supporting information.³⁵⁻³⁷ H_2O_2 dissociation is believed to occur over the Ag surface and probably follows the mechanism, suggested by Kazarnovsky³⁸ (Supporting Information). We can rationally assume that since tungsten oxide is acidic in nature; the basic aniline can be easily adsorbed onto the surface of acidic WO_3 through electrostatic interactions. During the oxidation process, dissociation of H_2O_2 over Ag generates superoxide ($\text{O}_2^{\bullet-}$), which ultimately produces peroxide species $\bullet\text{OOH}$, which is supposed to be the active species for this reaction (Supporting Information, eq (ii)). This $\bullet\text{OOH}$ then attacks the N-H bond of aniline, which is partially electropositive in nature after donating its electron pair to tungsten. We found phenyl hydroxyl amine and nitrosobenzene to be the intermediates for this reaction, which accords well with the reported literatures for the oxidative coupling of aniline with H_2O_2 .⁸ The oxidation reaction occurs step by step, where initially aniline oxidizes to phenyl hydroxyl amine, which further oxidizes to azobenzene. Finally azobenzene oxidizes to form azoxybenzene. To obtain insight into the reaction pathway, the reaction intermediates were separately subjected to oxidative coupling reaction using 2.5 wt% Ag/ WO_3 nanostructured catalyst. When phenyl hydroxyl amine was subjected to oxidation under the optimized condition, it produced azoxybenzene

within 16 h (Table 2, entry 9) and when azobenzene was subjected to oxidation, it produced azoxybenzene within 14 h (Table 2, entry 10). These experiments indicate that phenyl hydroxyl amine and azobenzene are the intermediates for this reaction for the formation of azoxybenzene. Interestingly when we added p-benzoquinone at optimized condition initially, we observed aniline conversion of 80% with 97 % azoxy benzene selectivity within just 16 h of reaction. Thereafter, in a separate reaction, equimolar of 2,6-di-tert-butyl-4-(4'-methoxyphenyl)phenoxy (DBMP) was added as a radical scavenger in the reaction medium to understand the possible formation of radical species. The reaction was almost suppressed under this condition and gave aniline conversion of ~17% after 24 h with major formation of azoxybenzene. All these results further suggest that addition of p-benzoquinone accelerates the reaction rate, whereas, DBMP retards it. This result further demonstrates the involvement of radical species in our system.

Reusability Test

We tested the reusability of the Ag/WO₃ nanostructured catalyst without further regeneration. The oxidative coupling of aniline was carried out with the reused catalyst under the same reaction condition. Activity of the recovered catalyst after four consecutive runs did not lead to any significant decline in its catalytic activity in terms of conversion and selectivity (Figure S4). After completion of the reaction, the solid catalyst was removed from the reaction mixture by filtration during hot condition and the reaction was allowed to proceed with the filtrate under the same conditions. The reaction was completely stopped after the removal of the catalyst. Another important finding is that the oxidation pathway does not involve homogeneous catalysis by dissolving tungsten or silver species. TEM image does not show any change compared to the initial morphology and particle size distribution (Fig. 5f). We also observed that the amount of Ag and W present in the spent catalyst after 4 reuses is

almost same with that of the fresh catalyst as estimated by ICP-AES, which further confirms the true heterogeneity of the catalyst. XPS also confirmed that almost no change was occurred in the metallic state of the silver before and after four reuses.

Conclusions

In summary, we have demonstrated a simple preparation method for the one pot synthesis of 2-5 nm Ag nanoparticles supported on nanocrystalline WO_3 . The catalyst was characterized by XRD, XPS, BET- surface area, ICP-AES, FT-IR, TGA, EXAFS, SEM and TEM. In the light of the findings, we can say that the Ag/WO_3 nanostructured catalyst serves as a highly selective heterogeneous catalyst for the one step selective oxidation of saturated primary N-H bonds of aniline to azoxybenzene with H_2O_2 as oxidant at room temperature. The oxidative coupling proceeds in a highly selective manner without the use of any external additives yielding an aniline conversion of 87% with 91% azoxybenzene selectivity. The significantly enhanced activity of our catalyst stems from the combination of the factors like: a) nanosize effect, the uniformly dispersed very small silver particles (~ 2 nm) generates more active sites for the reaction and b) the synergistic interaction between the ~ 2 -5 nm AgNPs and nanocrystalline WO_3 .

Acknowledgements

S.G. thanks UGC, S.S.A. thanks CSIR, India for the fellowship. R.B thanks CSIR, New Delhi for the financial support in the form of 12 FYP Project (CSC-0125, CSC 0117). Director, CSIR-IIP, is acknowledged for his support and encouragement. The authors thank Analytical

Section Division, CSIR-IIP. The XAFS measurements were performed at KEK-IMSS-PF with the approval of the Photon Factory Advisory Committee (project 2013G210).

Notes and References:

^a*Catalytic Conversion & Processes Division, CSIR-Indian Institute of Petroleum, Dehradun 248005, India*

^b*Department of Complexity Science and Engineering, Graduate School of Frontier Sciences, The University of Tokyo, Kashiwanoha, Kashiwa-shi, Chiba 277-8561, Japan*

Corresponding author. Tel.: +91 135 2525797; Fax: +91 135 2660202

E-mail addresses: raja@iip.res.in

† Electronic supplementary information (ESI) available.

1. J. Hu, T. W. Odom and C. M. Lieber, *Acc. Chem. Res.*, 1999, **32**, 435.
2. A. K. Geim and K. S. Novoselov, *Nature Mater.*, 2007, **6**, 183.
3. R. B. Laughlin, *Phys. Rev. Lett.*, 1983, **50**, 1395.
4. M. Law, J. Goldberger and P. Yang, *Annu. Rev. Mater. Res.*, 2004, **34**, 83.
5. S. J. Tauster, S. C. Fung and R. L. Garten, *J. Am. Chem. Soc.*, 1978, **100**, 170.
6. S. C. Catino and E. Farris, *Concise Encyclopedia of Chemical Technology* (Wiley, New York, **1985**), chap. VII.

7. (a) F. Hamon, F. Djedaini-Pilard, F. Barbot and C. Len, *Tetrahedron*, 2009, **65**, 10105; (b) E. R. Burkhardt and K. Matos, *Chem.Rev.*, 2006, **106**, 2617; (c) J. P. Adams, *J. Chem. Soc., Perkin Trans.*, 2002, **1**, 2586; (d) A. M. Tafesh and J. Weiguny, *Chem. Rev.*, 1996, **96**, 2035; (e) G. S. Kumar and D. C. Neckers, *Chem. Rev.*, 1989, **89**, 1915.
8. S. S. Acharyya, S. Ghosh and R. Bal, *ACS Sustainable Chemistry & Engineering.*, 2014, **2**, 584.
9. E. Buncl, *Can. J. Chem.*, 2000, **78**, 1251.
10. E. Buncl, *Acc. Chem. Res.*, 1975, **6**, 132.
11. R. W. White and W. D. Emmons, *Tetrahedron.*, 1962, **17**, 31.
12. H. E. Baumgarten, A. Staklis and E. M. Miller, *J. Org. Chem.* 1965, **30**, 1203..
13. E. Wenkert and B. Wickberg, *J. Am. Chem. Soc.* 1962, **84**, 4914.
14. H. Firouzabadi and Z. Mostafavipoor, *Bull. Chem. Soc. Jpn.* 1983, **56**, 914.
15. G.R. Howe and R.R. Hiatt, *J. org. chem.*, 1970, **35**, 4007.
16. Z. Zhu and J. H. Espenson, *J. Org. Chem.*, 1995, **60**, 1326.
17. E. B. Mel'nikov, G. A. Suboch and E. Y. Belyaev, *Zh. Org. Khim.*, 1995, **31**, 1849.
18. A. Defoin, *Synthesis*, 2004, 706.
19. C. F. Chang and S. T. Liu, *J. Mol. Catal A: Chem.*, 2009, **299**, 121.
20. T. Selvam and A. V. Ramaswamy, *Chem. Commun.*, 1996, 1215.
21. A. Grirrane, A. Corma and H. Garcia, *Science* 2008, **322**, 1661.
22. S. Cai, H. Rong, X. Yu, X. Liu, D. Wang, W. He, and Y. Li, *ACS Catal.*, 2013, **3**, 478.
23. H. M. Alizadeh and R. Tayebee, *J. Braz. Chem. Soc.*, 2005, **16**, 108.
24. (a) S. S. Acharyya, S. Ghosh, R. Tiwari, B. Sarkar, R. K. Singha, C. Pendem, T. Sasaki and R. Bal, *Green Chem.*, 2014, **16**, 2500; (b) S. Ghosh, S.S. Acharyya, S. Adak, L. N. S. Konathala, T. Sasaki and R. Bal, *Green Chem.*, 2014, **16**, 2826; (c) B. Sarkar, P. Prajapati, R. Tiwari, S. Ghosh, S. S. Acharyya, C. Pendem, R. K. Singha, L. N. S. Konathala, J. Kumar, T. Sasaki, and R. Bal, *Green Chem.*, 2012, **14**, 2600; (d) S. S. Acharyya, S. Ghosh and R. Bal, *Chem.Comm.*, 2014, **50**, 13311; (e) S.

Ghosh, S. S. Acharyya, R. Tiwari, B. Sarkar, R. K. Singha, C. Pendem, T. Sasaki, and R. Bal, *ACS Catal.*, 2014, **4**, 2169; (f) A. Shukla, R. K. Singha, T. Sasaki, and R. Bal, *Green Chem.*, DOI:10.1039/c4GC01664E.

25. E. A. Stern, M. Newville, B. Ravel, Y. Yacoby and D. Haskel, *Physica B:Condensed Matter*, 1995, **117**, 208.
26. M. Newville, P. Livins, Y. Yacoby, E. A. Stern and J. J. Rehr, *Phys. Rev. B*, 1993, **47**, 14126.
27. A. L. Ankudinov, B. Ravel, J. J. Rehr and S. D. Conradson, *Phys. Rev. B.*, 1998, **58**, 7565.
28. A. L. Ankudinov, A. I. Nesvizhskii and J. J. Rehr, *Phys. Rev. B.*, 2003, **67**, 115120.
29. B. Ravel, *J. Synchrotron Rad.*, 2001, **8**, 314.
30. D. C. Lim, I. Lopez-Salido and Y. D. Kim, *Surf. Sci.*, 2005, **598**, 96.
31. M. Breedon, P. Spizzirri, M. Taylor, J. Plessis, D. McCulloch, J. Zhu, L. Yu, Z. Hu, C. Rix, W. Wlodarski and K. Kalantar-zadeh, *Cryst. Growth & Des.*, 2010, **10**, 430.
32. W. Cheng, S. Dong and E. Wang, *Langmuir* 2003, **19**, 9434.
33. M.G. Fabra, P. Dunne, D. Grant, P. Gooden and E. Lester, *Chem. Eng. J.*, 2013, **226**, 22.
34. E. I. Ross-Medgaarden, W. V. Knowles, T. Kim, M. S. Wong, W. Zhou, C. J. Kiely and I.E. Wachs, *J. Catal.*, 2008, **256**, 108.
35. E. Saion, E. Gharibshahi and K. Naghavi, *Int. J. Mol. Sci.*, 2013, **14**, 7880.
36. J. Z. Guo, H. Cui, W. Zhou and W. Wang, *J. Photochem. Photobiol., A: Chem.* 2008, **193**, 89.
37. Y. Ono, T. Matsumura, N. Kitajima and S-I. Fukurumi, *J. Phys. Chem.* 1977, **81**, 1307.
38. A. M. Jones, S. Garg, D. He, A. N. Pham and T. D. Waite, *Environ. Sci. Technol.* 2011, **45**, 1428.

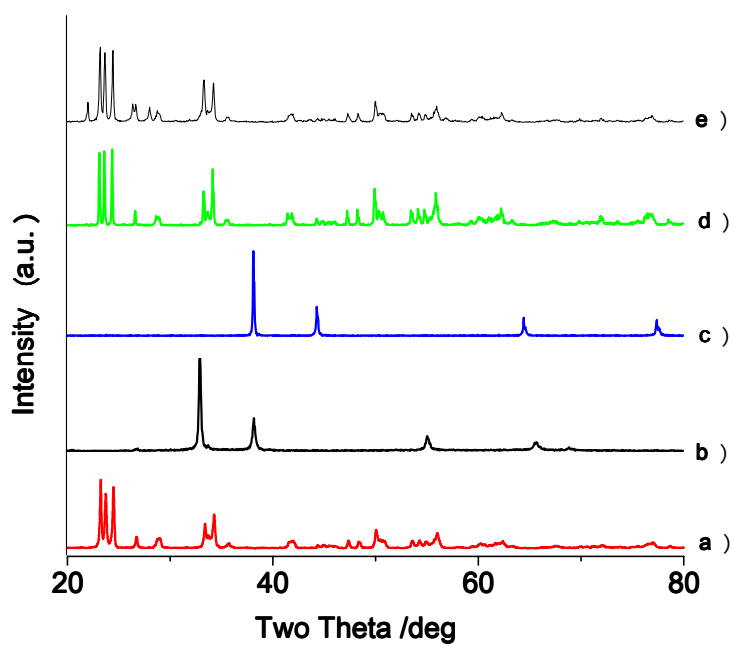


Fig. 1 XRD patterns of a) W (VI) Oxide, b) Ag (I) oxide, c), Ag (0), d) fresh Ag/WO₃ and e) spent Ag/WO₃.

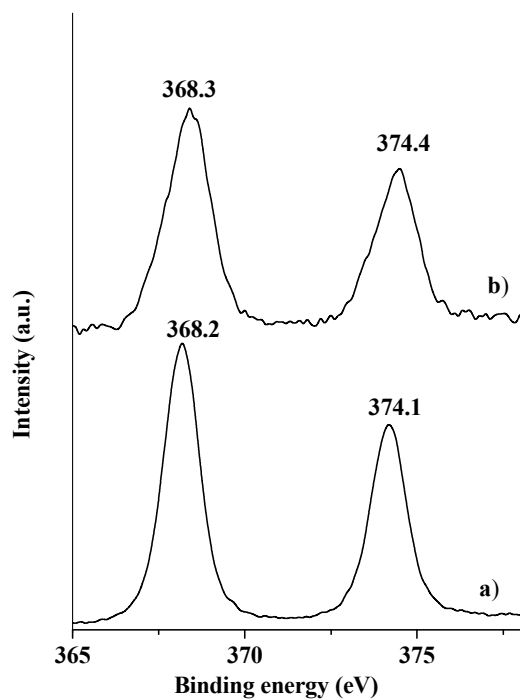


Figure 2. Ag 3d core level spectra a) fresh Ag/WO₃ catalyst and b) spent catalyst.

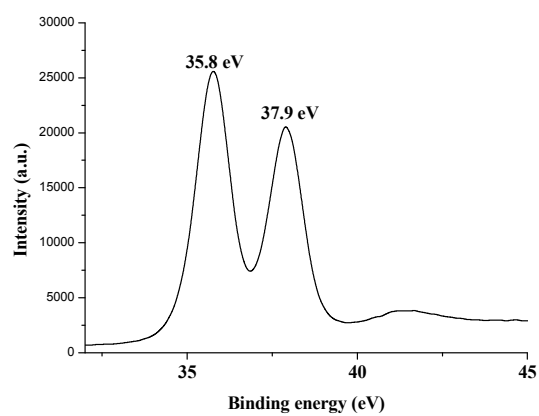


Figure 3. W4f_{7/2}, W4f_{5/2} core level spectra of the fresh Ag/ WO₃ catalyst.

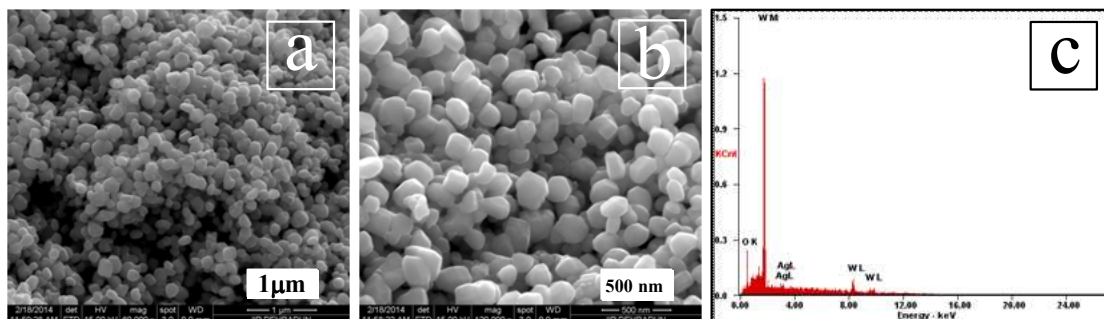


Figure 4. (a), (b) SEM and (c) SEM-EDX of Ag/WO₃ nanostructured catalyst

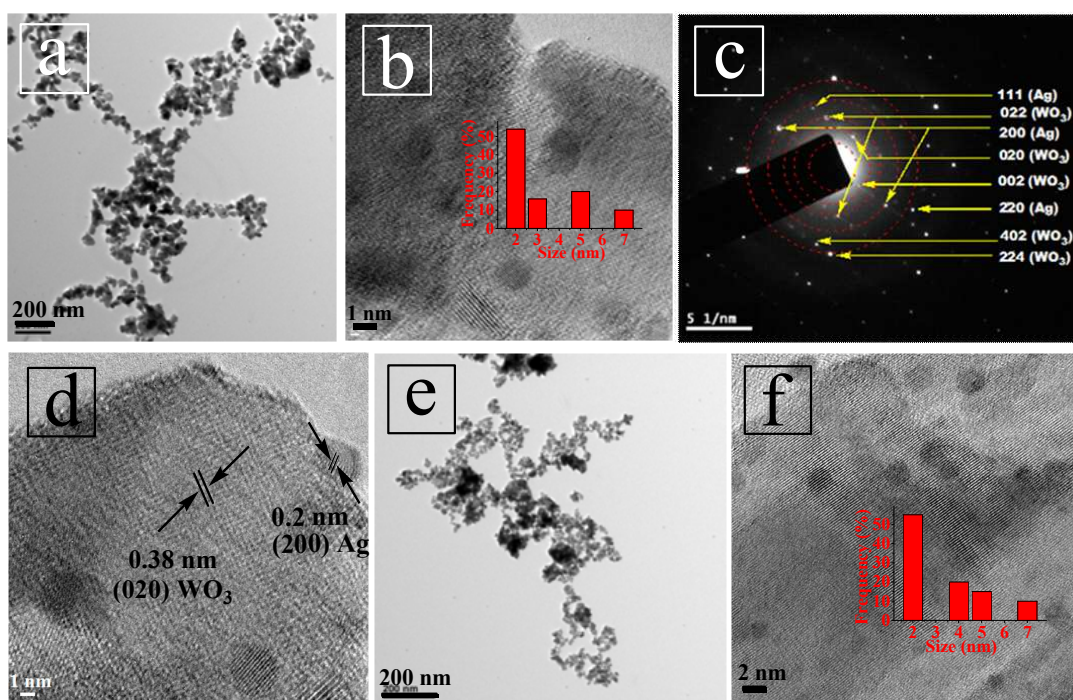


Figure 5. (a), (b) TEM image of fresh Ag/WO₃ nanostructure catalyst (inset Ag particle size distribution), (c) selected area electron diffraction image (SAED, d) lattice fringes and e), f) TEM image of used catalyst (inset Ag particle size distribution).

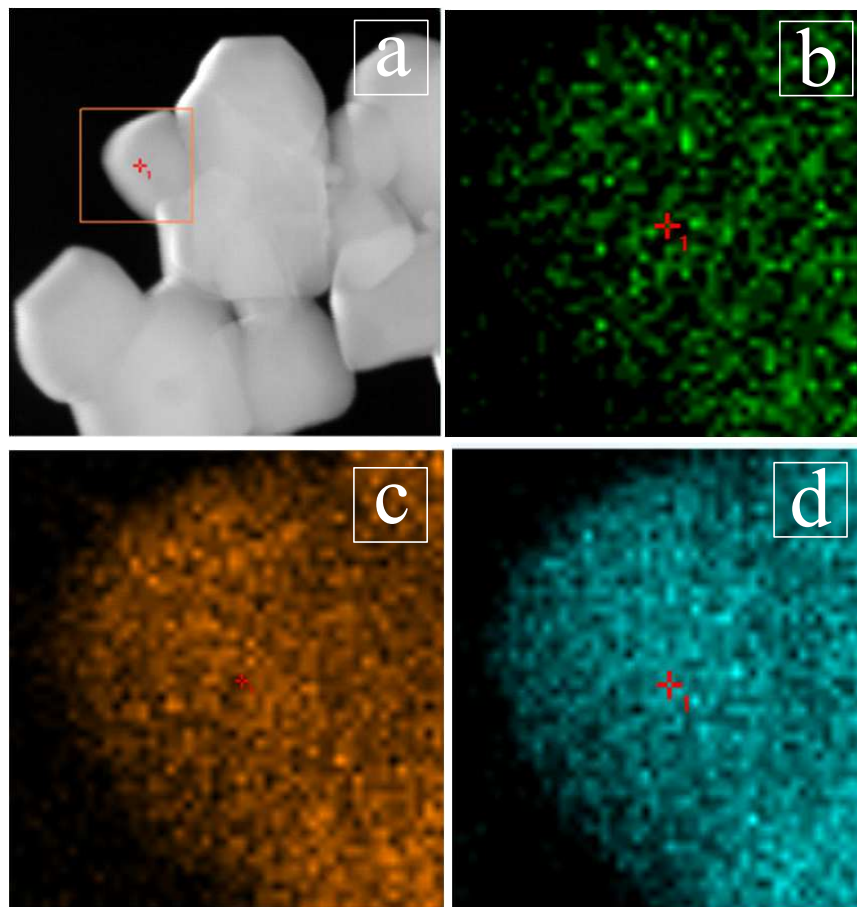


Figure 6. TEM elemental mapping of Ag/WO₃ catalyst a) TEM image, b) position of silver, c) position of oxygen and d) position of tungsten.

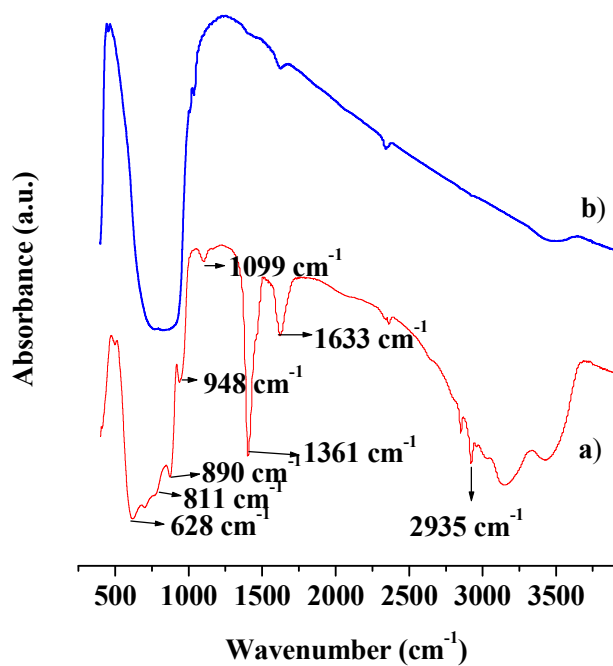


Figure 7. Infra-red spectra of a) uncalcined Ag/WO₃ catalyst and b) calcined catalyst.

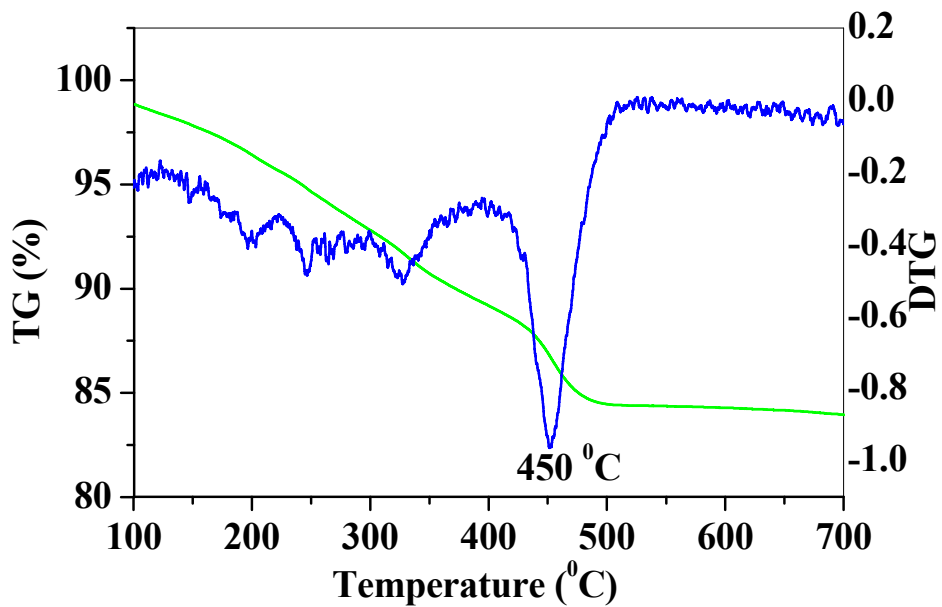


Figure 8. TG and DTG analyses of uncalcined Ag/ WO₃ catalyst.

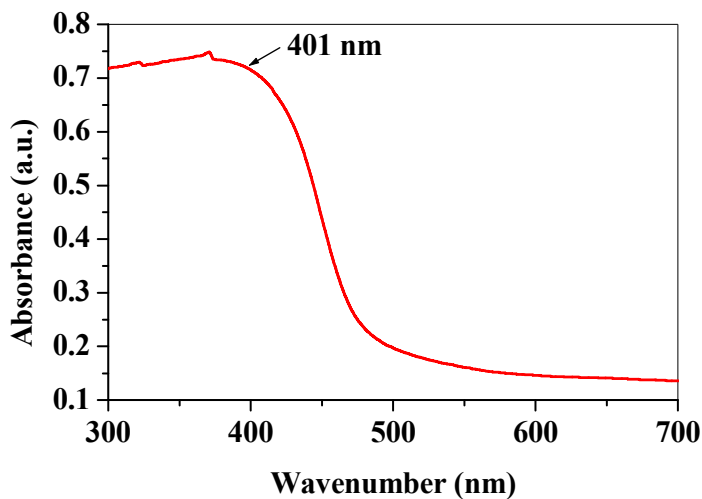


Figure. 9. UV-vis DRS spectrum Ag/ WO₃ nanostructured catalyst.

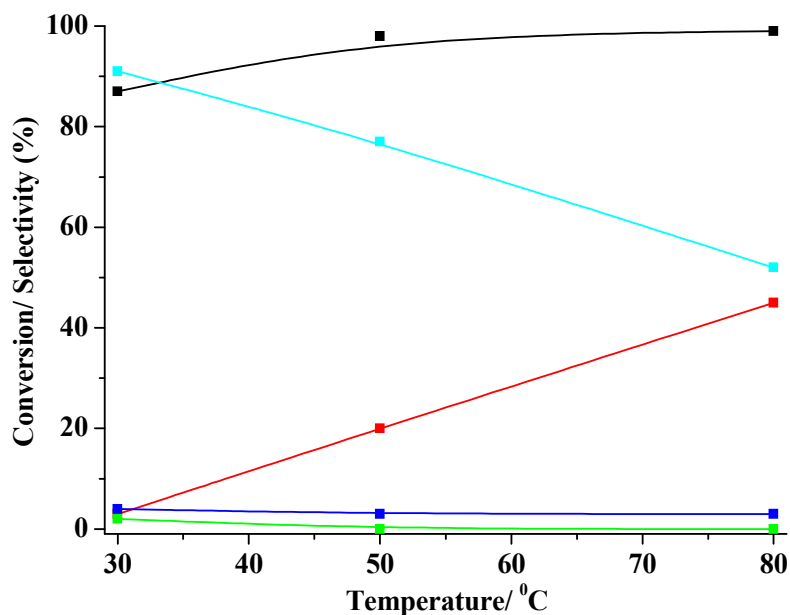


Figure. 10 Effect of temperature on aniline oxidation.

[■] Conversion of aniline; [■] Selectivity to nitrobenzene; [■] Selectivity to nitrosoaniline, [■] selectivity to azobenzene, [■] Selectivity to azoxybenzene. Reaction Condition: solvent= acetonitrile; aniline =1g; weight of catalyst = 0.10 g; aniline: H₂O₂ mole ratio =1:3; time = 24 h.

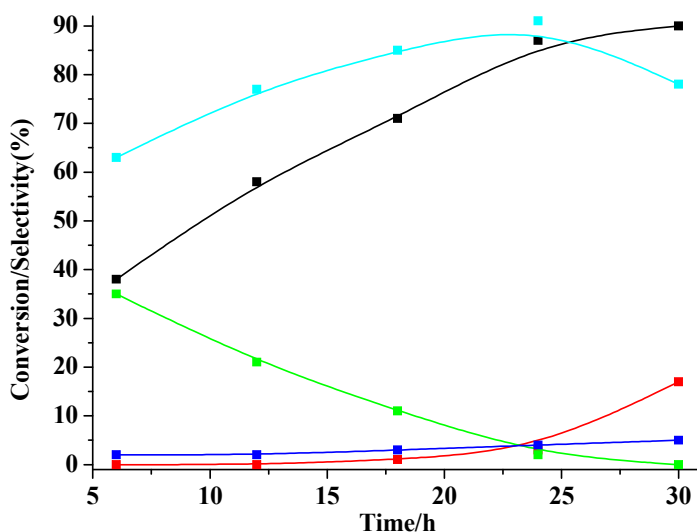


Figure. 11 Effect of time on aniline oxidation.

[■] Conversion of aniline; [■] Selectivity to nitrobenzene; [■] Selectivity to nitrosoaniline, [■] selectivity to azobenzene, [■] Selectivity to azoxybenzene. Reaction Condition: solvent= acetonitrile; aniline =1g; weight of catalyst = 0.10 g; substrate: H_2O_2 mole ratio =1:3; time = 24 h.

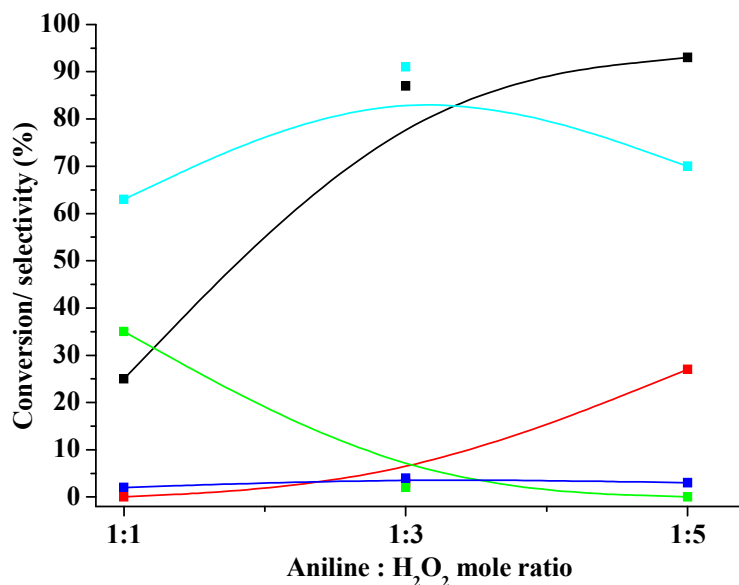


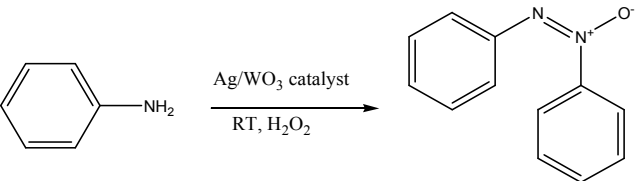
Figure. 12 Effect of aniline: H_2O_2 mole ratio on aniline oxidation.

[■] Conversion of aniline; [■] Selectivity to nitrobenzene; [■] Selectivity to nitrosoaniline, [■] selectivity to azobenzene, [■] Selectivity to azoxybenzene. Reaction Condition: solvent= acetonitrile; aniline =1g; weight of catalyst = 0.10 g; : H_2O_2 mole ratio =1:3; time = 24 h.

Table 1. EXAFS curve-fitting parameters at Ag–K-edge Fourier-filtered k^3 -weighted EXAFS functions

Catalyst	Path	R (10^{-1} nm)	CN	DW (10^{-5} nm ²)	Δk (10 nm ⁻¹)	ΔR (10^{-1} nm)	ΔE_0 (eV)	R _f (%)
Fresh	Ag-Ag	2.872±0.032	6.3±0.5	8.8±0.4	3 – 14	1.5–3.0	-1.1±0.7	0.79
Spent	Ag-Ag	2.873±0.031	7.7±0.6	9.4±0.4	3 – 14	1.0–3.0	1.8±0.6	1.04

EXAFS = extended X-ray absorption fine structure; CN= co-ordination number; R = bond length; DW: Debye-Waller factor; Δk : the range of wavenumbers used in the fitting; Δr : the range of bond distances used in the fitting; $S_0^2=0.95$, S_0^2 : amplitude reducing factor; ΔE_0 : shift of the edge-position; R_f: Reliability factor.

Table 2. Oxidative coupling of aniline to azoxybenzene^a


Entry	Catalyst	C _T ^b (%)	Selectivity S _P ^c (%)				Yield Y _A ^d (%)	Turn over Number (TON)	H ₂ O ₂ efficiency (%)
			Nitro benzene	Nitroso benzene	Azo benzene	Azoxy benzene			
1	Ag ^{com}	3.2	11	40.5	48.5	-	-	-	-
2	WO ₃ ^{com}	4.8	9	53	3	35	-	-	-
3	Ag ^{us}	27	14	27	59	-	-	-	-
4	WO ₃ ^{us}	21	9	34	-	57	12	-	4
5	Ag/WO ₃ ^{imp}	15	39	-	5	54	8.1	37.6	2.7
6	Ag/WO ₃ nano catalyst ^e	87	3	2	4	91	79.1	367.8	26.4
7	Ag/WO ₃ nano catalyst ^f	86	4	2	4	90	77.4	359.5	25.8
8	No Catalyst	0.3	-	-	-	-	-	-	-
9	Ag/WO ₃ nano catalyst ^g	99	-	-	5	95	94.0	436.9	31.3
10	Ag/WO ₃ nano catalyst ^h	99	-	-	-	99	98.0	455.3	32.7

^aReaction conditions: solvent (acetonitrile) = 10ml, substrate (aniline) = 1g, weight of the catalyst = 0.10g, silver loading = 2.5 wt%, reaction temperature = Room Temperature; time = 24h; aniline: H₂O₂ mole ratio = 1: 3; ^bC_T: conversion of aniline based upon the FID-GC results = [moles of aniline reacted/initial moles of aniline used] x 100; ^cS_P: selectivity of product calculated by total moles of product formed/total moles of aniline converted; ^dY_A (Yield of azoxybenzene) = conversion × selectivity/100; TON calculation ^e~Ag nanoparticles supported on WO₃; ^fcatalyst after 4 reuse; Ag/WO₃ nano catalyst ^g = when phenyl hydroxyl amine used as reactant, time = 16 h; Ag/WO₃ nano catalyst ^h = when azobenzene used as reactant, time = 14 h; com = Commercial; us = Bare Ag and WO₃ prepared by our method; imp = impregnation method.

Table 3. Activities of Ag/WO₃ nanostructure catalyst for the formation of azoxybenzenes via selective oxidation of different substituted anilines.

Entries	Substrate	C _T (%)	Product	Time h	Selectivity	Yield (%)
1		65		24	88	57.2
2		78		24	95	88.35
3		87		24	92	84.6
4		81		24	89	72.0
5		82		24	92	71.7
6		86		24	87	74.8

^aReaction conditions: Solvent (acetonitrile) = 10ml, substrate = 1g, weight of the Ag/WO₃ catalyst = 0.10g, silver loading= 2.5 wt%, time = 24 h; Aniline: H₂O₂ mole ratio = 1: 3.